Integrated Modeling of Natural (Hurricane) and Man-Made (Oil Spill) Disasters

C. Vipulanandan and B. Basirat
Texas Hurricane Center for Innovative Technology (THC-IT)
Department of Civil and Environmental Engineering
University of Houston, Houston, Texas 77204-4003
Tel: (713)-743-4278; Email: cvipulanandan@uh.edu; bbasirat@uh.edu

Abstract

With the increase in natural and man-made activities close to the coastal regions there is a need to develop integrated disaster models to predict the potential damages and prepare and enhance the resilience of the coastal communities. In this study, major constituents for the integrated model have been identified. Also 35 major offshore oil spill disasters around the world over the past 50 years have been analyzed where 30% were in the Gulf of Mexico. In order to demonstrate the combined effects of disasters, this study also investigated the effect of convection currents caused by hurricanes on oil spill.

$$\frac{dC}{dt} = f(C, x, y, z)$$
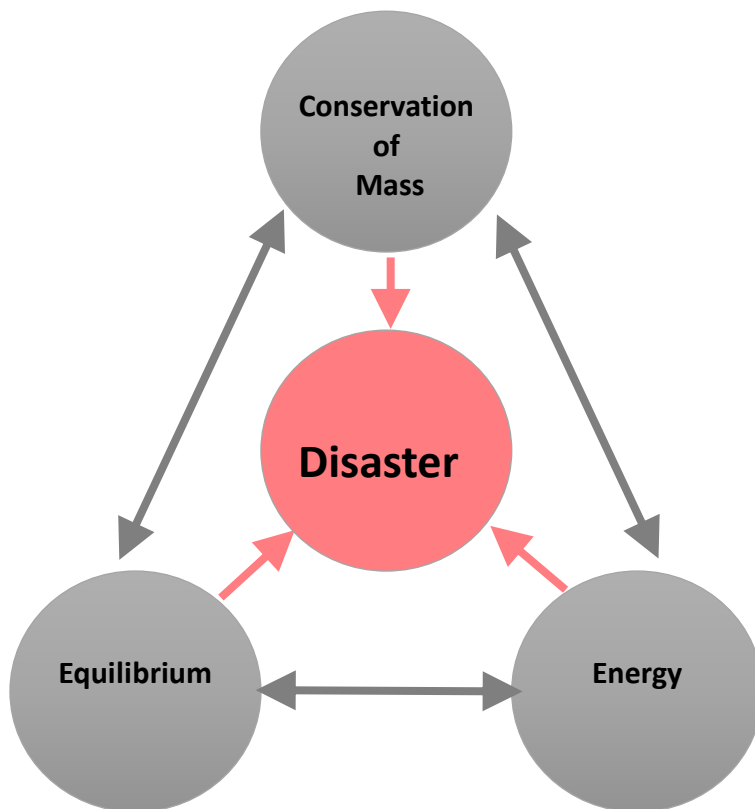
$$\sum p = m\ddot{x} = m\frac{d^2x}{dt^2} \qquad \sum F = Hurricane + Fire = K\left(\frac{dx}{dt}\right)^m + N\left(\frac{dC}{dt}\right)^n$$

Figure 1. Chart of combination of disaster

Introduction

Various types of crude oil are spilled into the ocean from tankers, offshore platforms, and drilling rigs and wells due to accidents. A summary of the major oil spills since 1967 are summarized in Table 1. (http://www.infoplease.com/ipa/A0001451.html). There were total of 35 major oil spill accidents around the world. About 30% of the accidents occurred in the Gulf of Mexico and half of them happened only in the last decade. Analyses of the accidents also indicated that about 15% of the oil spill accidents were combined with other disasters such as fire and hurricane.

Governing Equations

Man-made disaster (example oil spill) coupled with natural disasters (hurricanes, fire) will be controlled by the following governing equations (Fig. 1): (1) conservation of mass, (2) equilibrium and (3) conservation of energy. For example natural disaster such as hurricane (large focused energy) can add tremendous energy to the oil spill system by affecting both the dispersion of the oil (conservation of mass) and also the dynamic condition (equilibrium).

Table 1. Summary of 50 years il of oil spill around the world

Year	Location of oil spill	Name of Oil Spill	Remark
1967 March 18	**Cornwall, Eng.**	*Torrey Canyon*	38 million gallons crude oil.
1976 Dec. 15	**Buzzards Bay, Mass**	*Argo Merchant*	7.7 million gallons of fuel oil.
1977 April	**North Sea**		81 million gallons
1978 March 16	**off Portsall, France**	wrecked supertanker *Amoco Cadiz*	68 million gallons, causing widespread environmental damage over 100 mi of Brittany coast.
1979 June 3	**Gulf of Mexico** ✱		140 million gallons crude oil. Although it is one of the largest known oil spills.
1979 July 19	**Tobago**	*the Atlantic Empress and the Aegean Captain*	46 million gallons 41 million gallons.
1980 March 30	**Stavanger, Norway**		killing 123 oil workers
1983 Feb. 4	**Persian Gulf, Iran**		80 million gallons of oil.
1983 Aug. 6	**Cape Town, South Africa**	the Spanish tanker *Castillo de Bellver*	**Caught fire**, 78 million gallons of oil off the coast.
1988 July 6,	**North Sea off Scotland**		166 workers killed in **explosion** and **fire** on Occidental Petroleum's Piper Alpha rig in North Sea; 64 survivors. It is the world's worst offshore oil disaster.
1988 Nov. 10	**Saint John's, Newfoundland**	*Odyssey*	43 million gallons of oil.
1989 March 24	**Prince William Sound, Alaska**	tanker *Exxon Valdez*	10 million–plus gallons of oil.
1990 June 8	**off Galveston, Tex** ✱	*Mega Borg*	Released 5.1 million gallons of oil some 60 nautical miles south-southeast of Galveston as a result of an **explosion** and subsequent **fire** in the pump room.
1991 Jan. 23–27	**southern Kuwait**		240–460 million gallons of crude

			oil.
1991 April 11	**Genoa, Italy**	*Haven*	42 million gallons of oil.
1991 May 28	**Angola**	*ABT Summer*	15–78 million gallons of oil.
1992 March 2	**Fergana Valley, Uzbekistan**		88 million gallons of oil.
1993 Aug. 10	**Tampa Bay, Fla** *	Three ships collided, the barge *Bouchard B155,* the freighter *Balsa 37,* and the barge *Ocean 255.* The *Bouchard*	336,000 gallons of No. 6 fuel oil.
1994 Sept. 8	**Russia**		102,000 barrels.
1996 Feb. 15	**off Welsh coast**	supertanker *Sea Empress*	
1999 Dec. 12	**French Atlantic coast**	Maltese-registered tanker Erika	3 million gallons of heavy oil.
2000 Jan. 18	**off Rio de Janeiro**		343,200 gallons of heavy oil.
2000 Nov. 28	**Mississippi River south of New Orleans** *	oil tanker *Westchester*	567,000 gallons of crude oil.
2002 Nov. 13	**Spain**	*Prestige*	20 million gallons of oil remains underwater.
2003 July 28	**Pakistan**	The *Tasman Spirit,*	28,000 tons of crude oil.
2004 Dec. 7	**Unalaska, Aleutian Islands**	A major storm pushed the M/V *Selendang Ayu*	337,000 gallons of oil.
2005 Aug.-Sept	**New Orleans, Louisiana** *		7 million gallons of oil were spilled during **Hurricane Katrina** from various sources, including pipelines, storage tanks and industrial plants.
2006 June 19	**Calcasieu River, Louisiana** *		An estimated 71,000 barrels of waste oil were released from a tank at the CITGO Refinery on the Calcasieu River during a **violent rain storm.**
2006 July 15	**Beirut, Lebanon**		Between three million and ten million gallons of oil leaks into the sea, affecting nearly 100 miles of coastline.
2006 August 11	**Guimaras island, The Philippines**		530,000 gallons of oil.
2007 December 7	**South Korea**		2.8 million gallons of crude oil.
2008 July 25	**New Orleans, Louisiana** *		Hundreds of thousands of gallons of fuel.
2009 March 11	**Queensland, Australia**		52,000 gallons of heavy fuel and 620 tons of ammonium nitrate, a fertilizer, into the Coral Sea. About 60 km of the Sunshine Coast was covered in oil, prompting the closure of half the area's beaches.
2010 Jan. 23	**Port Arthur, Texas** *	The oil tanker Eagle Otome	462,000 gallons of crude oil. about 46,000 gallons were recovered and 175,000 gallons were dispersed.

| 2010 April 24 | **Gulf of Mexico** * | The *Deepwater Horizon* | A semi-submersible drilling rig, sank on April 22, after an April 20th explosion on the vessel. Eleven people died in the blast. When the rig sank, the riser—the 5,000-foot-long pipe that connects the wellhead to the rig—became detached and began leaking oil. In addition, U.S. Coast Guard investigators discovered a leak in the wellhead itself. As much as 60,000 barrels of oil per day were leaking into the water, threatening wildlife along the Louisiana Coast. Homeland Security Secretary Janet Napolitano declared it a "spill of national significance." BP (British Petroleum), which leased the *Deepwater Horizon,* is responsible for the cleanup, but the U.S. Navy supplied the company with resources to help contain the slick. Oil reached the Louisiana shore about 125 miles of coast. Oil had also reached Florida, Alabama, and Mississippi. It is the **largest oil spill in U.S. history** |

(http://www.infoplease.com/ipa/A0001451.html).

Case 1: Conservation of Mass

Mass transport is defined as the transport of a solute in a solvent. In each diffusion reaction (heat flow, for example, is also a diffusion process), the flux (of matter, heat, electricity, etc.) follows the general relation (John, 2007):

$$\text{Flux} = (\text{conductivity}) \times (\text{driving force})$$

(a) Heavy weight crude oil

The heavy-weight components are characterized by (Michel)

- Hydrocarbon compounds have more than 20 carbon atoms
- No loss by evaporation
- No water-soluble fraction
- Potential for bioaccumulation, via sorption onto sediments, otherwise not highly bioavailable
- Potential for chronic toxicity, they contain polynuclear aromatic hydrocarbons (phenanthrene, anthracene)
- Most of the components are waxes, asphaltenes, and polar compounds. They do not have any significant bioavailabilites or toxicities
- Long-term persistence in sediments, as tar balls, or asphalt pavements.

(b) Molar concentration of crude oil

Molar concentration comes from the following equation

$$molarity = molar\ concentration = \frac{amount\ in\ moles\ of\ solute}{volume\ of\ solution} = \frac{density}{molecular\ weigth}$$

Density of heavy crude oil and the molecular weight of crude oil is about 800-1000 kg/m3 and 400 gr/mol, respectively (Borges, 2009). By calculation the molar concentration of crude oil is about 2500 mol/m3.

(c) Diffusion and Temperature

Diffusion coefficient is a function of temperature (Hamoda, 1988):

Table 2. Diffusion at different temprature

Temperature (°C)	25	35	45
Diffusion coefficient (cm²/hr)	0.286	0.52	0.758

(d) Governing equations

The mass conservation for a mass transport problem can be written as (John S. Gulliver 2007).

$$\underset{\text{IN}}{\text{Flux rate}} - \underset{\text{OUT}}{\text{Flux rate}} + \underset{\text{rate}}{\text{Source}} - \underset{\text{rate}}{\text{Sink}} = \text{Accumulation}$$

1. **Diffusive flux rate**

Diffusion is defined as spreading due to gradient in concentrations

$$\underset{(g/s)}{\text{Diffusive flux rate}} = -\underset{(m^2/s)}{D} \quad \underset{(g/m^4)}{\frac{\partial C}{\partial x}} \quad \underset{(m)^2}{A_x} \tag{1}$$

2. **Convective flux**

In convective flux we will have mass carried by means of the velocity of the particles.

$$\begin{array}{ccccc} \text{Convective} & & \text{Velocity component} & & \text{Surface} \\ \text{flux rate} & = & \text{normal to surface} & \times\ \text{area} & \times\ \text{Concentration} \\ (g/s) & & (m/s) & (m^2) & (g/m^3) \end{array} \tag{2}$$

or

$$\text{Convective flux rate} = u\,A_x C$$

3. **Accumulation rate**

Accumulation rate is defined by the volume and concentration gradient

$$\underset{(g/s)}{\text{Rate of accumulation}} = \underset{(m^3)}{\overline{V}} \quad \underset{(g/m^3/s)}{\frac{\partial C}{\partial t}} \tag{3}$$

4. **Source and sink rates**

$$\text{Source} - \text{sink rate} = S \qquad \overline{V} \qquad\qquad (4)$$
$$\text{(g/s)} \qquad \text{(g/m}^3\text{/s)} \qquad \text{(m}^3\text{)}$$

(e) Mass balance on control volume

A mass balance through a box is based on whatever comes in must be either accumulate in the box, flux out from another side or react in source, sink terms (John S. G., 2007).
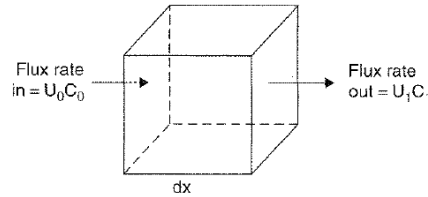

Figure 2. Illustration of the x-component of mass flux rate into and out of the control volume

For each spatial component of the cube we will have the following equation

$$\text{Flux rate (out} - \text{in})_x = \frac{\partial}{\partial x}(\text{flux rate})dx$$
$$\text{Flux rate (out} - \text{in})_y = \frac{\partial}{\partial y}(\text{flux rate})dy \qquad (5)$$
$$\text{Flux rate (out} - \text{in})_z = \frac{\partial}{\partial z}(\text{flux rate})dz$$

(f) Convective flux rate

Convective flux rate for each spatial component will be written as following

$$\text{Convective flux rate (out} - \text{in})_x = \frac{\partial}{\partial x}(u\,C\,A_x)\,dx = \frac{\partial}{\partial x}(u\,C)\,dx\,dy\,dz$$
$$\text{Convective flux rate (out} - \text{in})_y = \frac{\partial}{\partial y}(v\,C\,A_y)\,dy = \frac{\partial}{\partial y}(v\,C)\,dx\,dy\,dz \qquad (6)$$
$$\text{Convective flux rate (out} - \text{in})_z = \frac{\partial}{\partial y}(w\,C\,A_z)\,dz = \frac{\partial}{\partial z}(w\,C)\,dx\,dy\,dz$$

Summation of flux rates in all directions results in the total net convective flux

$$\text{Net convective flux rate} = \left[\frac{\partial}{\partial x}(u\,C) + \frac{\partial}{\partial y}(v\,C) + \frac{\partial}{\partial z}(w\,C)\right]dx\,dy\,dz \qquad (7)$$

(g) Diffusive flux rate

Diffusive flux rate for each spatial component will be written as following

$$\text{Diffusive flux rate (out} - \text{in})_x = \frac{\partial}{\partial x}\left(-D\frac{\partial C}{\partial x}A_x\right)dx = \frac{\partial}{\partial x}\left(-D\frac{\partial C}{\partial x}\right)dx\,dy\,dz$$
$$\text{Diffusive flux rate (out} - \text{in})_y = \frac{\partial}{\partial y}\left(-D\frac{\partial C}{\partial y}A_y\right)dy = \frac{\partial}{\partial y}\left(-D\frac{\partial C}{\partial y}\right)dx\,dy\,dz \qquad (8)$$
$$\text{Diffusive flux rate (out} - \text{in})_z = \frac{\partial}{\partial z}\left(-D\frac{\partial C}{\partial z}A_z\right)dz = \frac{\partial}{\partial z}\left(-D\frac{\partial C}{\partial z}\right)dx\,dy\,dz$$

Summation of flux rates in all directions results in the total net diffusive flux

$$\text{Net diffusive flux rate} = -\left[\frac{\partial}{\partial x}\left(D\frac{\partial C}{\partial x}\right) + \frac{\partial}{\partial y}\left(D\frac{\partial C}{\partial y}\right) + \frac{\partial}{\partial z}\left(D\frac{\partial C}{\partial z}\right)\right]dx\,dy\,dz \tag{9}$$

(h) Control volume mass balance

By combining equations (3), (4), (7) and (9) in mass balance equation and substituting $\overline{V} = dxdydz$ and moving the diffusive flux terms to the right hand side we will have

$$\frac{\partial C}{\partial t} + \frac{\partial}{\partial x}(u\,C) + \frac{\partial}{\partial y}(v\,C) + \frac{\partial}{\partial z}(w\,C)$$
$$= \left[\frac{\partial}{\partial x}\left(D\frac{\partial C}{\partial x}\right) + \frac{\partial}{\partial y}\left(D\frac{\partial C}{\partial y}\right) + \frac{\partial}{\partial z}\left(D\frac{\partial C}{\partial z}\right)\right] + S \tag{10}$$

The convective transport term can be expanded as following

$$\frac{\partial}{\partial x}(u\,C) = u\frac{\partial C}{\partial x} + C\frac{\partial u}{\partial x}$$
$$\frac{\partial}{\partial y}(v\,C) = v\frac{\partial C}{\partial y} + C\frac{\partial v}{\partial y} \tag{11}$$
$$\frac{\partial}{\partial z}(w\,C) = w\frac{\partial C}{\partial z} + C\frac{\partial w}{\partial z}$$

If the flow is considered to be incompressible then we have (according to continuity equation)

$$\rho\left(\frac{\partial u}{\partial x} + \frac{\partial v}{\partial y} + \frac{\partial w}{\partial z}\right) = 0 \tag{12}$$

By summation of equations (11) and using equation (12) we will have

$$\frac{\partial}{\partial x}(u\,C) + \frac{\partial}{\partial y}(v\,C) + \frac{\partial}{\partial z}(w\,C) = u\frac{\partial C}{\partial x} + v\frac{\partial C}{\partial y} + w\frac{\partial C}{\partial z} \tag{13}$$

By substituting equation (13) in (10) and more simplifications we will get equation (14). It is assumed that the diffusion coefficient is constant in all directions (isotropic).

$$\frac{\partial C}{\partial t} + u\frac{\partial C}{\partial x} + v\frac{\partial C}{\partial y} + w\frac{\partial C}{\partial z} = D\left(\frac{\partial^2 C}{\partial x^2} + \frac{\partial^2 C}{\partial y^2} + \frac{\partial^2 C}{\partial z^2}\right) + S \tag{14}$$

(i) Difference between diffusion and dispersion

Diffusion is due to gradient in concentrations (equation (1)) whereas dispersion is due to pore to pore variation in velocity, velocity variation within the pores and spreading due to source strength, source location, local flow pattern and knowledge regarding geological heterogeneities defined as

$$Dispersion\ flux\ rate = D_M\frac{\partial C}{\partial x}A_x \tag{15}$$

Where $D_M = \alpha . v_a$, v_a is pore velocity which is equivalent to "u" in previous equations and α is dispersivity coefficient.

(j) Solution of the 3D convection-dispersion, diffusion equation

By considering dispersion and using index notation equation (14) will be

$$\underbrace{\frac{\partial}{\partial x_i}\left(D_{ij}\frac{\partial C}{\partial x_j}\right)}_{\text{Dispersion and diffusion}} - \underbrace{v_{a,i}\frac{\partial C}{\partial x_i}}_{\text{Advective in/outflow}} + \underbrace{S_n}_{\substack{\text{Source/sink (decay,}\\\text{sorption, etc.)}}} = \underbrace{\frac{\partial C}{\partial t}}_{\text{Change in storage}} \tag{16}$$

The equation (16) is the most general equation of diffusion considering diffusion, convection and source and sink. By introducing "Peclet number", the significance of diffusion, convection or both can be distinguished lead to a better solution or assumption for solving equation (16).

(1) Peclet number

The Peclet number (Jean Claude Eugène Péclet, 1793 – 1857)) (Pe) is a ratio of convection to diffusion term. The higher the Peclet number, the more important is convection and the lower the Peclet number the more important is the diffusion. The range of this number will emphasis the importance of convection and diffusion (Cushman-roisin, 2012).

$$\frac{advection}{diffusion} = \frac{u\frac{\partial c}{\partial x}}{D\frac{\partial^2 c}{\partial x^2}} = \frac{u\frac{C}{L}}{D\frac{C}{L^2}} = \frac{uL}{D}$$

If Pe $\ll$ 1 which means Pe $<$ 0.1, diffusion dominates the convection term is significantly smaller than the diffusion term. Therefore, the convection term is ignorable (v $\partial c/\partial x$). By dropping the convection term, the equation (14) in 1 dimensional (y direction) can be simplified to

$$\frac{\partial C}{\partial t} = D_y\frac{\partial^2 C}{\partial x^2} + S \tag{17}$$

If Pe $\gg$ 1 which means Pe $>$ 10, convection dominates the diffusion term is significantly smaller than the convection term. Therefore, the diffusion term is ignorable (D $\partial^2 c/\partial x^2$). By dropping the diffusion term, the equation (14) in 1 dimensional (y direction) can be simplified to

$$\frac{\partial c}{\partial t} + u\frac{\partial c}{\partial x} = 0 \quad \rightarrow \quad c(x,t) = c_0(x-ut) \tag{18}$$

If Pe $=1$ in practice it means 0.1 $<$ Pe $<$10, the convection and diffusion terms are important simultanously, and neither process dominates over the other. No approximation to the equation can be justified, and the full equation must be utilized.

(2) Analytical Solution

Time dependent convection diffusion with source

Equation (19) is a time dependent convection diffusion source in which the time dependent source is included the solution for this equation is shown in equation (20) which satisfied the boundary conditions (Cushman-roisin, 2012).

$$\frac{\partial c}{\partial t} + v\frac{\partial c}{\partial y} = D\frac{\partial^2 c}{\partial y^2} + Kc \tag{19}$$

The boundary condition including concentration at y = ∞ is equals to zero

$$c(y,t) = \frac{M}{\sqrt{4\pi Dt}}\exp(-\frac{(y-vt)^2}{4Dt} + Kt) \tag{20}$$

The source term "kc" is a function of first order term of concentration.

(3) Numerical Model

Oil has been applied at center in a circular manner at the middle of an elliptical domain. 4 cases were investigated including one dimensional model categorized in 1) small scale and 2) large scale. And a three dimensional model in 3) small scale and 4) large scale. Figure 3 and 4 are the meshing for 3-D large scale and small scale, respectively.
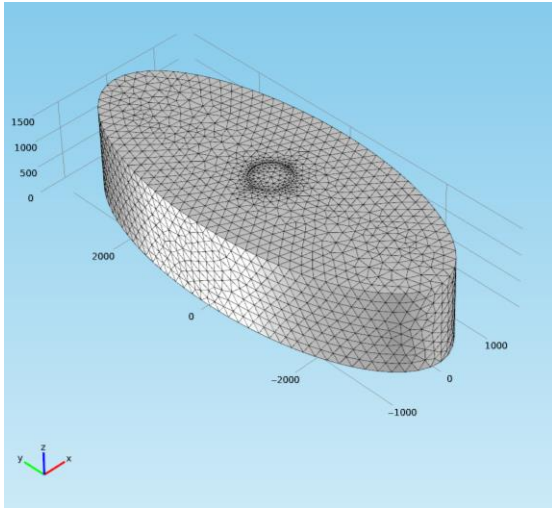

Figure 3. Tetrahedral elements Maximum 200 m and minimum 126 m
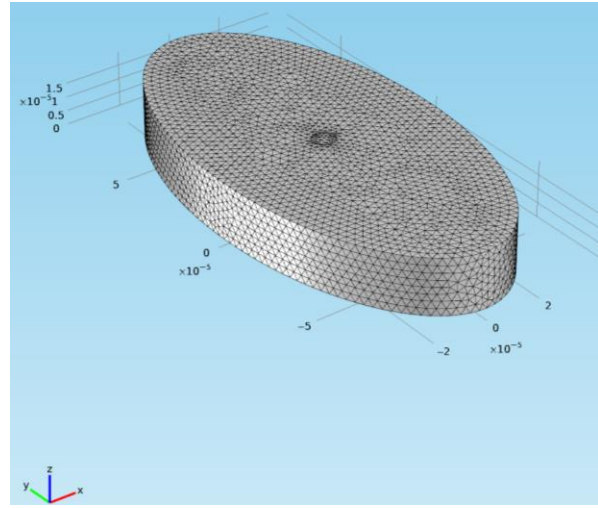

Figure 4. Tetrahedral elements Maximum 0.3e-5 m and minimum 2.88E-6 m

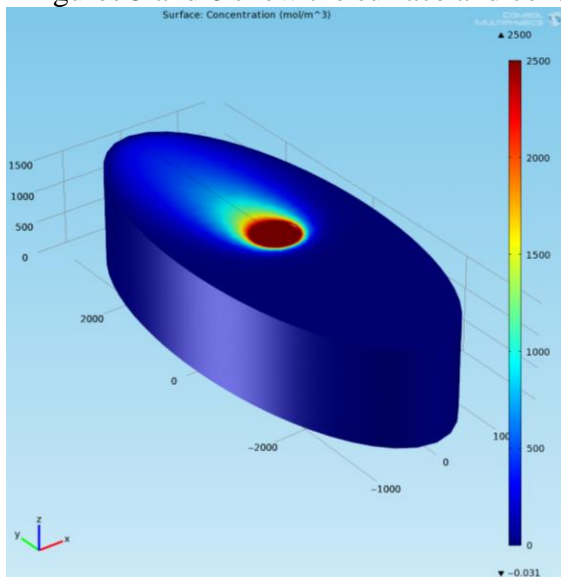Figures 5 and 6 show the surface and contours for concentration for 3 dimensional large scale.

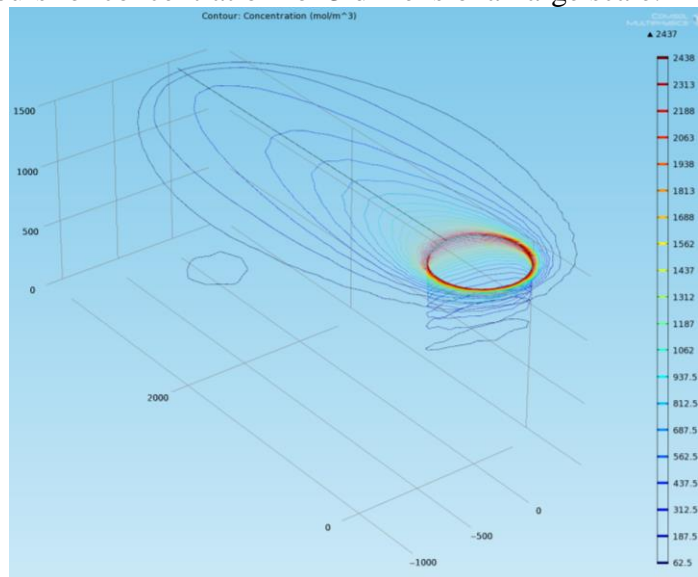**Figure 5. Surface concentration**

Figure 6. Contour lines of concentration

The path on which the 3D model was investigated is shown in figure 7, which is located along y axis.
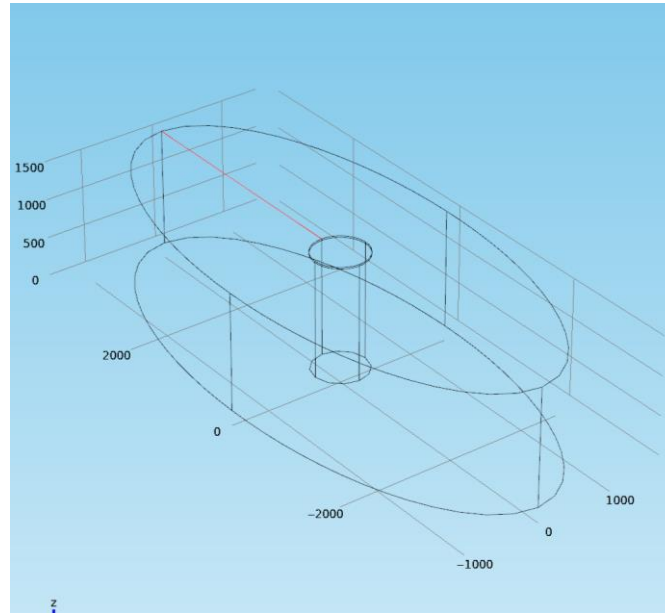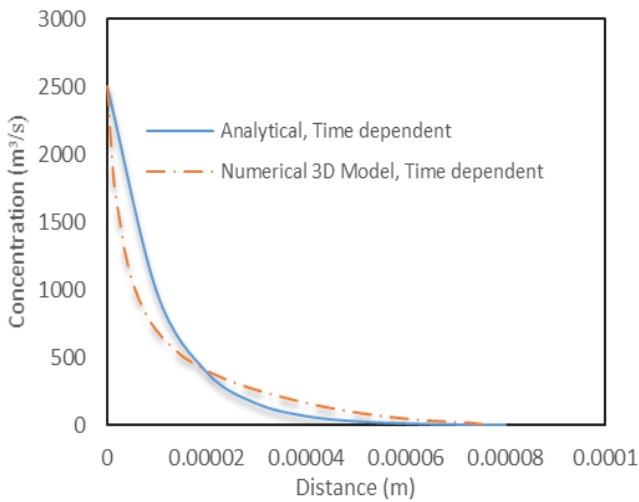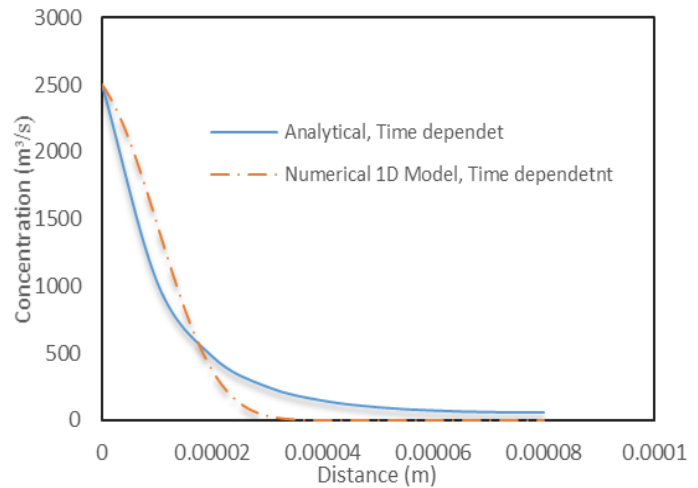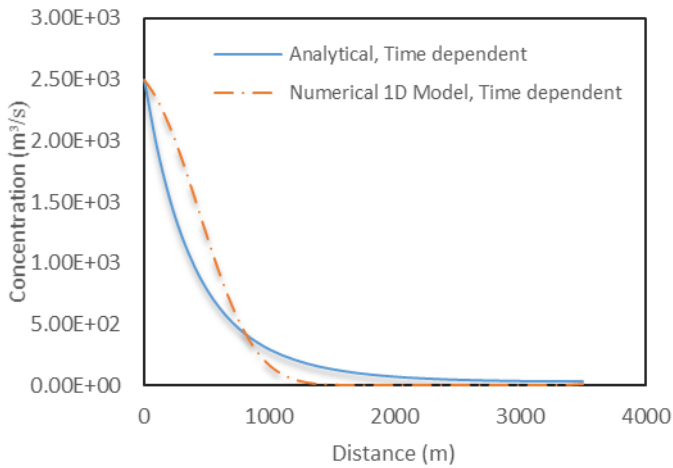
I-9

Figure 7. Path in 3D large scale

The 4 cases described before, was analyzed and the results of numerical with the analytical solution were compared and the comparisons are shown figures 8 through 11.
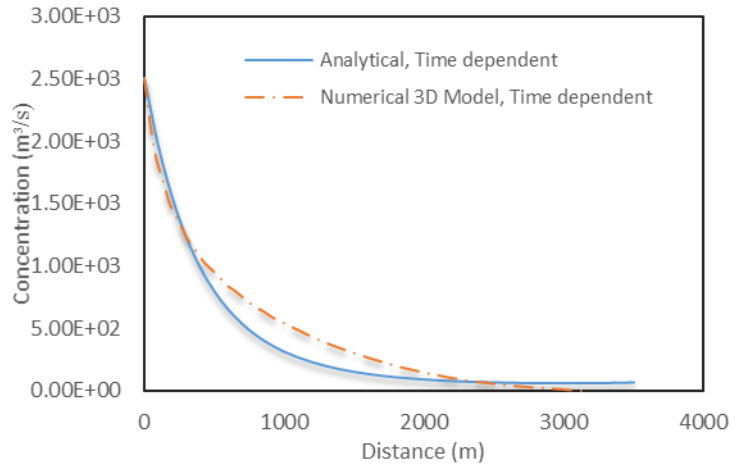

**Figure 8. Pe = 15.2, t = 0.1 s,
3D small scale model**

**Figure 9. Pe = 15.2, t= 0.02 s,
1D small scale model**

Figure 10. Pe = 17.5, t = 700 s,
1D large scale model

Figure 11. Pe = 17.5, t = 600 s,
3D large scale model

Figures 12 and 13 are the variation of concentration under various time and velocity versus distance, respectively. By decreasing the duration of problem, the concentration vanishes later. For example at t= 0.02 the concentration vanishes at y = 3e-5 m while at t = 0.014 the concentration vanishes at y = 8e-5 m. As shown in figure 13, the higher convection effect due to higher velocity of the domain leads to higher spread of concentration over the domain. Therefore, in the hurricane while we have the oil spill it will be more disperse and the more damages will be expected.
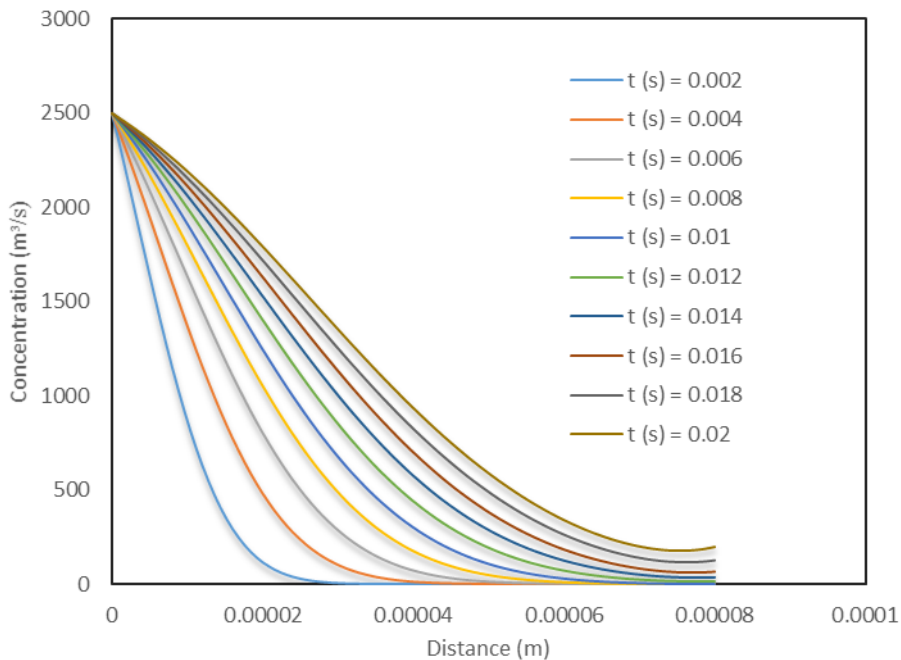

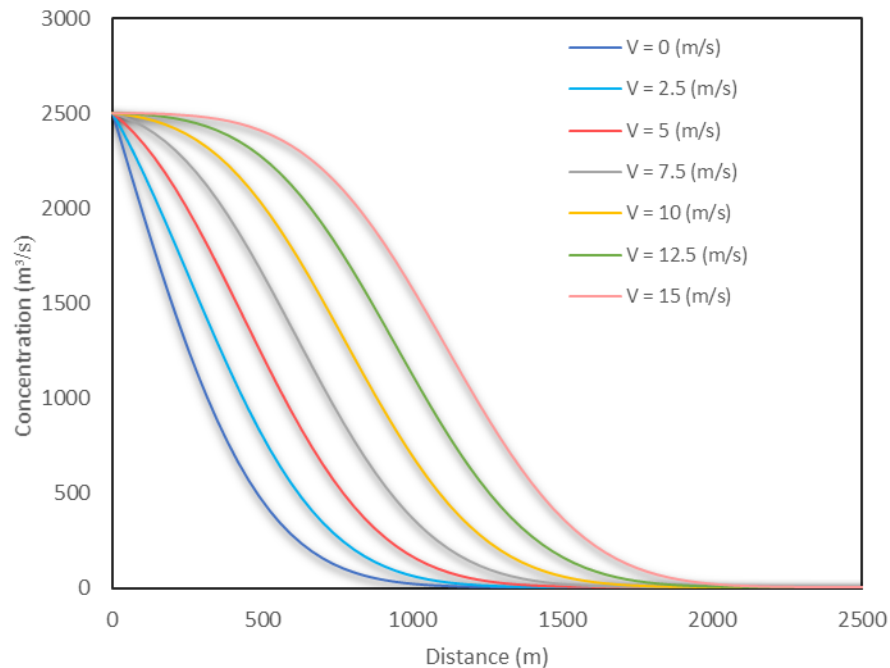**Figure 12. Numerical 1D small scale model, Pe = 3.8**

Figure 13. Numerical 1D Large scale model

Conclusion

An integrated model was proposed to include the natural disaster with the man-made disasters. Also the effect of hurricane was applied to the conservation of mass relationship (convection term) and the distribution of oil in 1D and 3D models were investigated. The convection velocity affected the distribution (variation of oil concentration with distance) of the oil.

References

[1]. Borges, B. (2009). Natural Surfactants from Venezuelan Extra Heavy Crude Oil - Study of Interfacial and Structural Properties.

[2]. Cushman-roisin, B. (2012). Environmental Transport and Fate Chapter 2. Diffusion – Part 5: With convection.

[3]. Michel, J. (n.d.). Oil Behavior and Toxicity Chapter 2 . Oil Behavior and Toxicity.

[4]. http://www.infoplease.com/ipa/A0001451.html

[5]. John S. G. (2007). Introduction to Chemical Transport in the Environment Chapter 2. The diffusion equation

[6]. http://www.thelambertfirm.com/u-s-supreme-court-refuses-stop-bp-oil-spill-payments-now/

Subsidence in Houston Observed by Satellite Radar Instruments

Hyongki Lee and Ning Cao

National Center for Airborne Laser Mapping
Department of Civil and Environmental Engineering,
University of Houston, Houston, TX

Subsidence can be caused by a diverse set of human activities and natural processes, including mining of coal, withdrawal of ground water, petroleum, and melting of permafrost. More than 80 percent of the identified subsidence in the Nation results from underground water pumping. The increasing development of urban area and need of water resources threaten to exacerbate existing land subsidence problems and initiate new ones (Galloway et al., 1999). Local collapse may damage buildings, roads, and utilities, and either impair or totally destroy them, leading to expensive repairs. The Nation Research Council estimated that annual costs in the United States from flooding and structural damage caused by land subsidence exceeded $125 million (National Research Council, 1991). Thus, it becomes vital to monitor the land subsidence in high spatial and temporal resolutions to be able to assess its impacts on civil infrastructure. In this study, we focus on mapping land deformation over the Houston area that has been caused by the withdrawal of groundwater, oil and gas using an innovative satellite radar imaging technique.

Differential interferometric synthetic aperture radar (DInSAR) has already been proven to be a useful technique for measuring ground displacement. Among various multitemporal DInSAR techniques, persistent (or permanent) scatterer InSAR (PSInSAR) has been widely used in a variety of cases due to its high accuracy and resistance to temporal and spatial decorrelations. The basic idea of PSInSAR is to find and analyze the pointwise time-coherence targets with long-time-span differential interferograms. One major drawback of PSInSAR technique is the low spatial density of PSs, especially for rural areas without man-made structures. Unlike dominant persistent scatterers, the distributed scatterer (DS) pixel normally contains a coherent sum of individual small scatterers. The interference of these small scatterers causes the variation in the returned signal, which leads to temporal and geometrical decorrelations. The distributed scattering mechanism usually covers several pixels with similar statistically homogeneous behaviors. Hence, it is possible to get sufficient coherence by processing these DSs statistically.

Several PSInSAR methods have been proposed to improve the PS network density by extracting information from the distributed targets. For example, the Small Baseline Subset (SBAS) method aims at reducing the geometrical decorrelation by analyzing the interferograms with short time interval and small normal baselines. The StaMPS (Stanford Method for Persistent Scatterers) method utilizes the spatial and temporal correlation of the phase, combining with proper filtering and unwrapping methods, to extract the deformation signal at more locations. One merit of SBAS and StaMPS method is that the deformation time series can be obtained without prior knowledge of the deformation model. Many efforts have been made to improve the spatial density of PSs by jointly processing PS and DS. SqueeSAR applies the phase triangulation algorithm to get the best estimates of the N phases associated with the deformation of DS from N(N-1)/2 off-diagonal interferometric phases of the coherence matrix. Then, this optimized phase is used to perform the conventional PSInSAR processing. Quasi-PS (QPS) technique uses

spatial coherence as weight in the estimate process to extract information from partially coherent targets. An improved PS approach is also proposed to use homogenous patches to estimate the gradient for deformation velocity and residual DEM errors. Then the deformation velocity is obtained by performing an integration process. A major disadvantage of this method is that the deformation pattern must be known.

The distributed scatterer interferometry approaches mentioned above only concern one dominant scatterer (One PS) and small homogeneous scatterers. In reality, it is possible to have two or more dominant scatterers (Multiple PSs) within the same resolution pixel. This multiple dominant scatterering mechanism can occur in rural areas and some urban areas with low spatial resolution. Extracting information from DS with multiple dominant scatterers is difficult because of the constructive and destructive interference between them. Especially for images with low spatial resolution, it is more likely that multiple dominant scatterers exist in the same pixel. Usually, average filtering is implemented in DInSAR process to improve the SNR. This average filtering process would decrease the resolution and enhance the interference. The multiple dominant scatterering mechanism has already been analyzed and corresponding signal models are also proposed in the literatures. But this higher-order PS method assumes that all scatterers within the same pixel experience the same deformation.

In order to deal with the multiple dominant scatterering mechanism, a phase-decomposition-based PSInSAR method is proposed in this study. For the sake of simplicity, we name this approach as PD-PSInSAR. The general idea is to use Eigen-decomposition to estimate the phases corresponding to the multiple dominant scatterers, and then to implement these estimated phases in conventional PSInSAR process. Even though all the phases for the multiple dominant scatterers are estimated, we only use the primary PS (the dominant scatterer with the largest eigenvalue and best coherence) to do the PSInSAR processing. Comparing with the existing DS techniques, the proposed PD-PSInSAR method is expected to have the following advantages:
1) More number of PSs can be detected because the multiple dominant scatterers are included,
2) Because the phase of the primary dominant scatterer can be distinguished from the secondary dominant scatterer, the interference between different dominant scatterers are mitigated, and the obtained phases are expected to have better coherence.
3) Simplicity and portability. The decomposition process is simple and straightforward without the need for significant changes in the conventional PSInSAR technique. The estimated phases can be utilized as the input of other DS techniques.

This PD-PSInSAR technique is used to estimate the land deformation over the Houston area using ENVISAT ASAR data spanning from 2004 to 2010. Comparison between the conventional, SqueeSAR, and PD-PSInSAR techniques verifies that the proposed PD-PSInSAR method can detect more PSs and provide better coherences. The deformation map reveals that the northwestern part of Houston has significant subsidence over the past six years, which is consistent with the estimates from published GPS measurements. Our subsidence hazard map can be used as a basis for mitigation efforts to reduce its damage to the civil infrastructure.

References
1. Galloway, D., D.R. Jones, and S.E. Ingebritsen, Land Subsidence in the United States, U.S. Geological Survey Circular, 1182, 1999.

2. National Research Council, Mitigating losses from land subsidence in the United States, National Academy Press, Washington, DC, 1991.